IJASRM
International Journal of Advanced Scientific Research and Management, Volume 3 Issue 7, June 2018
www.ijasrm.com
ISSN 2455-6378

Investigation of Impact in Smart Grid Disturbances on the Output of Solar Photovoltaic System

Yogesh Mehta [1], Ravindra Prakash Gupta [2] and O. S. Lamba [1]

[1] Department of Electronics and Communications Engineering, Gyan Vihar University, Jaipur, India

[2] Department of Electronics and Communications Engineering, Manda Institute of Tech., Bikaner, India

Abstract

This paper presents the study of impact of grid disturbances on the output of the solar PV energy in the smart grid. The disturbances due to the operations such as feeder tripping/reclosing, switching on/off of the resistive load, switching on/off the capacitor banks and switching on/off the inductive-resistive load has been considered. The voltage on the PCC and current injected by the solar PV system into the grid has been captured for the proposed study. The voltage is decomposed using the Stockwell transform and S-matrix is obtained. This S-matrix is used to obtain the amplitude curve and sum absolute values curve which is used for the detection of the voltage variations at point of common coupling. The variations in the output power of the solar PV system are directly monitored.

Keywords: *Grid disturbances, Smart Grid, Solar PV system, Stockwell Transform*

1. Introduction

Smart grid (SG) is an electricity network which intelligently integrates the actions of all the connected generators including conventional and distributed generators (DG), users and consumers in order to efficiently deliver sustainable, economic and secure electricity supply to consumers. This smart grid have innovative products and services together with intelligent monitoring, control, communication, and self-healing technologies in order to (i) provide the integration and operation of generators of all sizes and technologies (ii) allow consumers to play an active role in optimizing the operation of the system (iii) significantly reduce the environmental impact of the whole electricity supply system and (iv) preserve or improve the level of system quality of service, reliability and security [Enrico, Lorenzo, Alireza and Antonello, 2015].

The renewable energy (RE) sources are a promising alternative which help in reducing the emission of green house from electricity generation and produces environment friendly energy to meet out the future energy demand. These energy sources are expected to take a leading role in the future transition from a centralized to distributed generation scheme. Recently these sources are integrated to the smart grid. Solar photovoltaic energy is gaining popularity day by day. The disturbances caused in the smart grid due operations of the equipments, loads and feeders affects the output of these sources. In [Mahela and Ola, 2016], authors presented a discrete wavelet transform based study to investigate the impacts of grid disturbances such as switching of resistive and inductive loads, tripping of feeders feeding the consumers, outage of wind generator and synchronization of wind generator with the utility grid on the system parameters such as voltage and current at point of common coupling (PCC) as well as output of the wind generator. In [Sharma, Ola and Mahela, 2015], authors presented a discrete wavelet transform based study to investigate the impacts of grid disturbances such as switching of resistive and inductive loads, tripping of feeders feeding the consumers, outage of generator and synchronization of generator with the utility grid on the system parameters such as voltage and current at PCC as well as output of the solar PV modules. Various smart grid technologies and algorithms have been reported in the literature. Real et al. [Real, Arce and Bordons, 2014], presented an extended distributed model predictive control (DMPC) framework and its applications to a smart grid with the help of a case study to solve a combined environmental and economic dispatch problem. A smart home test bed to bridge the gap from traditional power systems to modernized smart grids has been reported in [Hu, Li and Chen, 2015]. [Chanda and De, 2014], proposed an optimization model to maximize social welfare by

standardizing the operating conditions with an overall improvement of dynamic stability of power markets in view of the smart grid communication technologies. The role of users in demand side management of smart grids with the help of a smart design has been presented in [Goulden, Bedwell, Rennick, Rodden and Spence, 2014]. A direct load control (DLC) method based on multi objective particle swarm optimization algorithm used for the load control in smart grids has been reported in [Evora, Hernandez and Hernandez, 2015]. [Karimi, Namboodiri and Jadliwala, 2015], presented a study of smart meter message concatenation problem to efficiently concatenate multiple small smart metering messages arriving at data concentrator units in order to reduce protocol overhead resulting in network utilization. A wide area measurement based dynamic stochastic optimal power flow control algorithm using the adaptive critical designs to achieve a high penetration level of intermittent renewable energy into the smart grids has been proposed by the authors in [Liang, Venayaga and Harley, 2012]. [Milioudis, Andreou and Labridis,2012], presented a method that deals with exact location of high impedance faults in the smart grids. A comparative analysis of tertiary control systems for smart grids using the flex street model has been reported in [Claessen, Molderink, Bakker, Toersche and Broek, 2014].

Hence, based on the above reviews this chapter has considered Stockwell transform which is more efficient compared to the discrete wavelet transform to study the impacts of disturbances on the output of the solar PV system in the smart grid caused due to the operations such as feeder tripping, feeder reclosing, switching on/off the resistive load, switching on/off the resistive-inductive load and switching on/off the capacitor bank. The study has been carried out in the MATLAB/Simulink environment using the IEEE-13 bus test system as the smart grid.

This paper is organized into six sections. Introduction is presented in the Section 1. The proposed smart grid model used for the study of impacts of grid disturbances on the output of solar PV system and voltage at PCC has been described in the section 2. Section 3 details the proposed methodology used for the study. The simulation results are presented in the section 4. The conclusions drawn based on the proposed study are presented in the section 5.

2. The Proposed Test System of Smart Grid

This section describes the test system which has been utilized as smart grid incorporated with solar photovoltaic (PV) energy system. This is used for the detection of various types of faults in the presence of the solar PV system. An IEEE-13 bus test system is modelled as a smart grid for the proposed study. The original system is a 60 Hz, 5 MVA, operating with the voltage levels of 4.16 kV and 0.48 kV. This system has the balanced and unbalanced loads and any RE source is not integrated to the original test system. The test system is modified to incorporate the solar PV system on the bus 680 of test system as illustrated in Fig. 1. Bus 680 is considered as point of common coupling (PCC). The solar PV system are connected to the test system at PCC through transformer XSPV. The loads connected to the test system at various buses are same as in the original test system. The distributed loads are connected at the middle of the respective distribution line of the test system. All the feeders of proposed test system have the configuration 601 of the original IEEE-13 system. Lengths of line segments are same as that in the original test system. The proposed test system of smart grid is connected to the conventional generator using a substation transformer. The transformer connected between the nodes 633 and 634 is named as XFM-1. This transformer is used to step down the voltage from 4.16 kV to 0.48 kV and bus 634 is maintained at voltage level of 0.48 kV. Technical details of transformers are provided in the Table 1. A three phase circuit breaker is used to represent the switch between the nodes 671 and 692 of the test system.

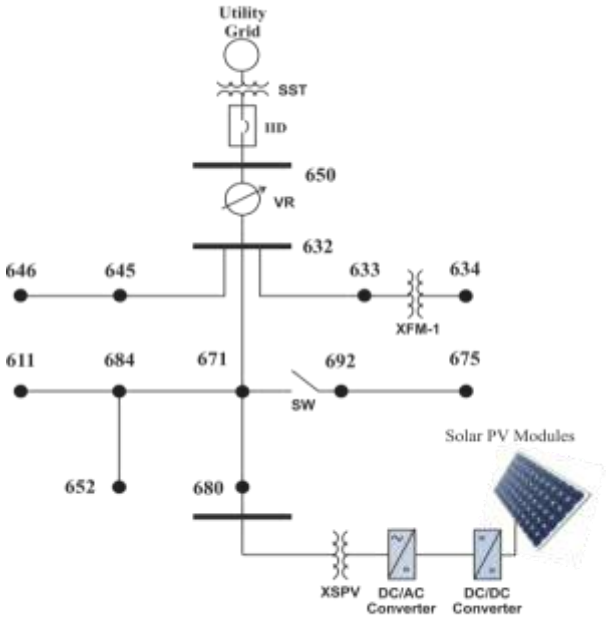

IEEE-13 bus test system modeled as smart grid

Table 1: Transformer Data of the Test System

Transformer	Voltage LV winding	Voltage HV winding	R (pu)	X pu)
SST	4.16 kV	115 kV	0.011	0.080
XFM-1	0.48 kV	4.16 kV	0.011	0.080
XSPV	260 V	4.16 kV	0.001	0.030

IJASRM
International Journal of Advanced Scientific Research and Management, Volume 3 Issue 7, June 2018
www.ijasrm.com
ISSN 2455-6378

3. Proposed algorithm for the study of impact of grid disturbances on the output of RE sources in the smart grid

The proposed detection algorithm for the study of impact of grid disturbances on the output of RE sources in the smart grid has been implemented with the following steps.

- The voltage signal is captured at PCC. The current and power injected by the RE sources are captured. These parameters are plotted with respect to the time and deviations from the standard values are recorded.
- The voltage signal captured at PCC is decomposed using S-transform to obtain S-matrix. The sampling frequency of 1.92 kHz is used and sampled over a period of 60 cycles.
- The S-transform based plots such as amplitude-time curve and sum absolute values curve are obtained from the S-matrix.
- Impact of disturbances on the output of RE sources has been investigated from the plots mentioned above.

3.1 Stockwell's Transform

The short time Fourier Transform of a signal h(t) is defined by the following relation.

$$STFT(\tau, f) = \int_{-\infty}^{+\infty} h(t)g(\tau - t)e^{-j2\pi ft}dt$$

where τ and f denote the time of spectral localization and Fourier frequency respectively, and $g(t)$ denote a window function. The S transform can be derived from the above equation by replacing the window function $g(t)$ with the Gaussian function as shown below.

$$g(t) = \frac{|f|}{\sqrt{2\pi}} e^{-\frac{f^2t^2}{2}}$$

Then the S-transform is defined as

$$S(\tau, f) = \int_{-\infty}^{+\infty} h(t) \frac{|f|}{\sqrt{2\pi}} e^{\frac{f^2(\tau-t)^2}{2}} e^{-j2\pi ft}dt$$

Hence, the S transform is a special case of STFT with Gaussian window function. If the window of S-transform is wider in time domain, S transform can provide better frequency resolution for lower frequency. While the window is narrower, it can provide better time resolution for higher frequency. The output of the S-transform is matrix known as S-matrix. The information related to the frequency and amplitude of the signal can be derived from the S-matrix

4. Solar Photovoltaic Power Generation: Simulation Results

The solar PV system of capacity 1 MW has been switched on at bus 680 of the smart grid test system shown in Fig. 4.1. The operations of feeder, capacitor banks and loads have been carried out at 10^{th} cycle to study the effect of grid disturbances on the output of solar PV system. The simulation results are detailed in the following subsections.

4.1 Feeder Tripping

The solar PV system of capacity 1 MW has been switched on at the bus 680 of the test system and continuously injecting power into the smart grid test system. The feeder comprising of buses 692 and 671 has been tripped at 10^{th} cycle. The voltage of phase-A at PCC, current injected into the grid at PCC by solar PV system and active power injected by the solar PV system in to the smart grid has been captured and their plots are shown in Figs. 2 (a), (b) and (c) respectively. It is observed from the Fig. 2 (a) that significant changes do not occur in the voltage at PCC. Slight deviations in the current waveform are observed as shown in Fig. 2 (b). The power deviations of 10 kW have been observed for a period of 4 cycles as shown in Fig. 2 (c).

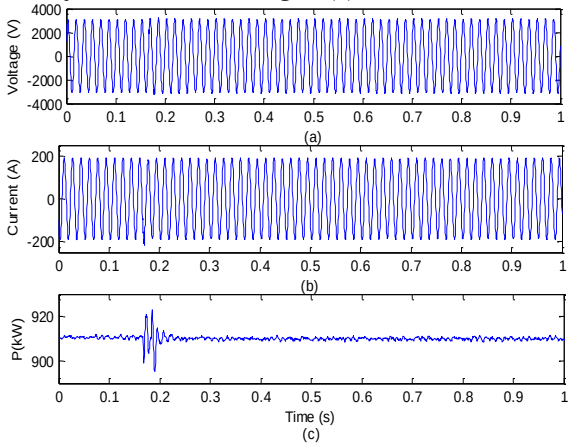

Fig. 1. (a) Voltage at PCC (b) current injected into the grid (c) active power flow with feeder tripping in the presence of solar PV power generation.

The amplitude curve and sum absolute values curve obtained from the S-matrix of the voltage during the feeder tripping are shown in Figs. 3 (a) and (b) respectively. The increase in the magnitude of amplitude curve after feeder tripping as shown in Fig. 3 (a) indicates that the voltage slightly increases with low magnitude voltage variations. These changes have not been detected in the voltage waveform. The high magnitude of the sum absolute values curve at the time of feeder tripping also indicates the presence of disturbances in the voltage waveform. Hence, disturbances are observed in the voltage at PCC, current and power injected by the solar PV system into the smart grid.

IJASRM
International Journal of Advanced Scientific Research and Management, Volume 3 Issue 7, June 2018
www.ijasrm.com
ISSN 2455-6378

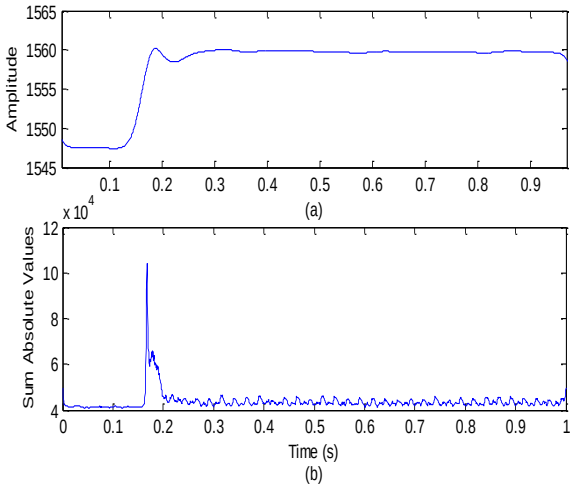

Fig. 2. Feeder tripping (a) amplitude curve obtained from S-matrix (b) sum absolute values curve obtained from S-matrix.

4.2 Feeder Reclosing

The solar PV system of capacity 1 MW has been switched on at the bus 680 of the test system and continuously injecting power into the smart grid test system. The feeder comprising of buses 692 and 671 is kept opened initially and reclosed at 10^{th} cycle. The voltage of phase-A at PCC, current injected into the grid at PCC by solar PV system and active power injected by the solar PV system in to the smart grid has been captured and their plots are shown in Figs. 4 (a), (b) and (c) respectively. It is observed from the Fig. 4 (a) that significant changes occur in the voltage at PCC due to feeder reclosing. Slight deviations in the current waveform are also observed as shown in Fig. 4 (b). The power deviations of 40 kW have been observed for a period of 10 cycles as shown in Fig. 4 (c).

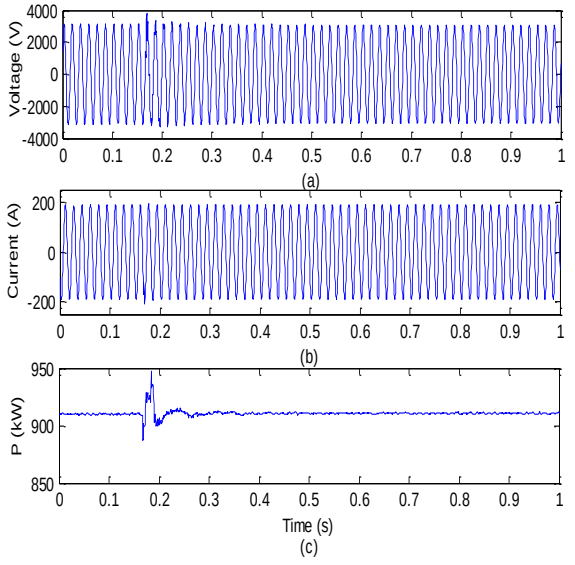

Fig. 3. (a) Voltage at PCC (b) current injected into the grid (c) active power flow with feeder reclosing in the presence of solar PV power generation.

The amplitude curve and sum absolute values curve obtained from the S-matrix of the voltage during the feeder reclosing are shown in Figs. 5 (a) and (b) respectively. The decrease in the magnitude of amplitude curve after feeder reclosing as shown in Fig. 5 (a) indicates that the voltage slightly decreases with low magnitude voltage variations. High magnitude of the sum absolute values curve at the time of feeder reclosing also indicates the presence of disturbances in the voltage waveform. Hence, disturbances are observed in the voltage at PCC, current and power injected by the solar PV system into the smart grid during the reclosing of the feeder in the smart grid.

4.3 Switching off the Resistive Load

The solar PV system of capacity 1 MW integrated to the smart grid test system at the bus 680 and continuously injecting power into the smart grid test system has been switched off at 10^{th} cycle. A resistive load of capacity 1155 kW initially connected to the smart grid at PCC has been switched off at 10^{th} cycle from start of the simulation. The voltage of phase-A at PCC, current injected into the grid at PCC by solar PV system and active power injected by the solar PV system in to the smart grid has been captured during the event of switching off the resistive load and their plots are shown in Figs. 6 (a), (b) and (c) respectively. It is observed from the Fig. 6 (a) that significant changes do not occur in the voltage at PCC due to switching off the resistive load. Further, the significant changes in the current waveform are also not observed as shown in Fig. 6 (b). The power deviations of 5 kW have been observed for a period of 3 cycles as shown in Fig. 6 (c). Hence, the changes during the switching off the resistive load are not significant.

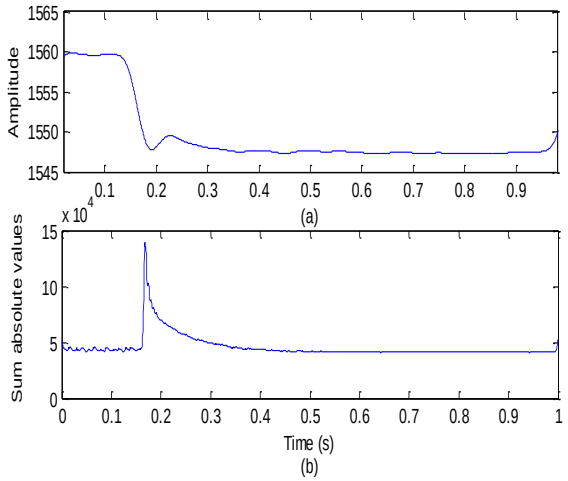

Fig. 4. Feeder reclosing (a) amplitude curve obtained from S-matrix (b) sum absolute values curve obtained from S-matrix

IJASRM
International Journal of Advanced Scientific Research and Management, Volume 3 Issue 7, June 2018
www.ijasrm.com
ISSN 2455-6378

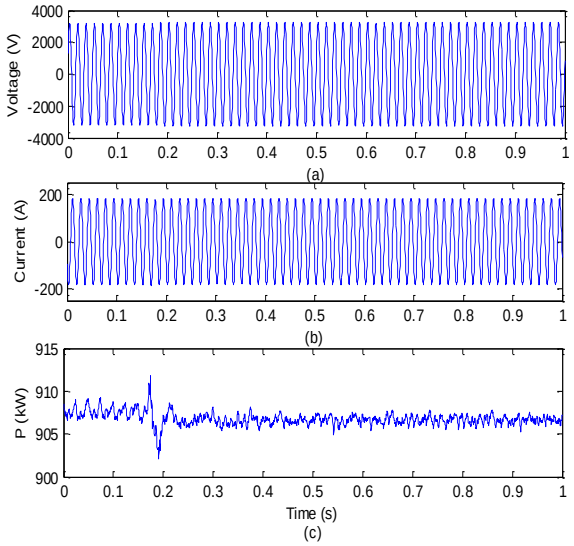

Fig. 5. (a) Voltage at PCC (b) current injected into the grid (c) active power flow with switching off the resistive load in the presence of solar PV power generation.

The amplitude curve and sum absolute values curve obtained from the S-matrix of the voltage during the switching of the resistive load are shown in Figs. 7 (a) and (b) respectively. The increase in the magnitude of amplitude curve after switching off the resistive load as shown in Fig. 7 (a) indicates that the voltage increases along with low magnitude voltage variations. High magnitude of the sum absolute values curve at the time of switching off the resistive load also indicates the presence of disturbances in the voltage waveform for short duration. Hence, disturbances are observed in the voltage at PCC and power injected by the solar PV system into the smart grid during the switching off the resistive load in the smart grid.

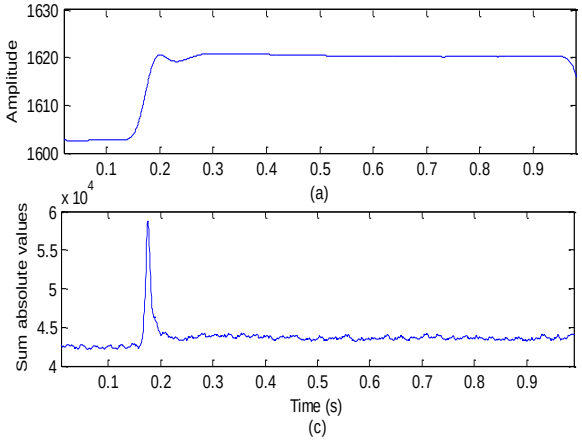

Fig. 6. Switching off the resistive load (a) amplitude curve obtained from S-matrix (b) sum absolute values curve obtained from S-matrix

4.4 Switching on the Resistive Load

The solar PV system of capacity 1 MW has been switched on at the bus 680 of the test system and continuously injecting power into the smart grid test system. A resistive load of capacity 1155 kW switched on at 10th cycle from start of the simulation and connected to the smart grid at PCC. The voltage of phase-A at PCC, current injected into the grid at PCC by solar PV system and active power injected by the solar PV system in to the smart grid has been captured during the event of switching on the resistive load and their plots are shown in Figs. 8 (a), (b) and (c) respectively. It is observed from the Fig. 8 (a) that significant changes visible by naked eye do not occur in the voltage at PCC due to switching on the resistive load. Further, the significant changes in the current waveform are also not observed as shown in Fig. 8 (b). The power deviations of 15 kW have been observed for a period of 5 cycles as shown in Fig. 8 (c). Hence, the changes during the switching on the resistive load are not significant in voltage and current but significant in the power generated by solar PV system.

The amplitude curve and sum absolute values curve obtained from the S-matrix of the voltage during switching on the resistive load are shown in Figs. 9 (a) and (b) respectively. The increase in the magnitude of amplitude curve after switching off the resistive load as shown in Fig. 9 (a) indicates that the voltage increases along with low magnitude voltage variations. High magnitude of the sum absolute values curve at the time of switching of the resistive load also indicates the presence of disturbances in the voltage waveform for short duration. Hence, disturbances are observed in the voltage at PCC and power injected by the solar PV system into the smart grid during the switching on the resistive load in the smart grid. The nature of voltage variations is similar during the cases of switching on and off the resistive load.

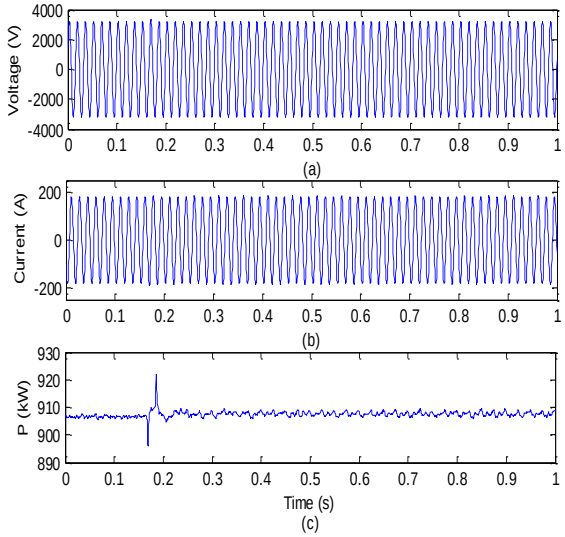

Fig. 7. Switching on the resistive load in the presence of solar power generation (a) voltage at PCC (b) current injected by solar PV system into the smart grid (c) power injected by solar PV system into the smart grid.

IJASRM
International Journal of Advanced Scientific Research and Management, Volume 3 Issue 7, June 2018
www.ijasrm.com
ISSN 2455-6378

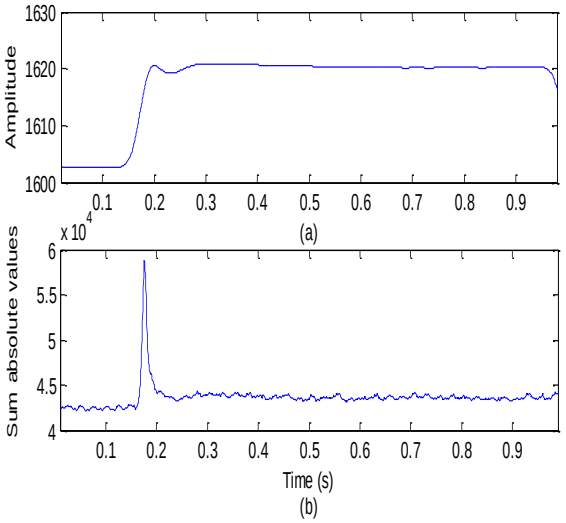

Fig. 8. Switching on the resistive load in the presence of solar PV system (a) amplitude curve obtained from S-matrix (b) sum absolute values curve obtained from S-matrix

4.5 Switching off the Inductive-Resistive Load

The solar PV system of capacity 1 MW integrated to the smart grid test system at the bus 680 and continuously injecting power into the smart grid test system. An inductive-resistive load of capacity 1155 kW and 1660 kVAr initially connected to the smart grid at PCC has been switched off at 10th cycle from start of the simulation. The voltage of phase-A at PCC, current injected into the grid at PCC by solar PV system and active power injected by the solar PV system in to the smart grid has been captured during the event of switching off the inductive-resistive load and their plots are shown in Figs. 10 (a), (b) and (c) respectively. It is observed from the Fig. 10 (a) that small changes occur in the voltage at PCC due to switching off the inductive-resistive load. Further, the current magnitude slightly decreases as shown in Fig. 10 (b). The power deviations of 10 kW have been observed for a period of 8 cycles as shown in Fig. 10 (c). It is also observed that power output of the solar PV system also decreases by an amount of 5 kW after switching off the inductive-resistive load.

The amplitude curve and sum absolute values curve obtained from the S-matrix of the voltage during the switching off the inductive-resistive load are shown in Figs. 11 (a) and (b) respectively. The increase in magnitude of amplitude curve after switching off the inductive-resistive load as shown in Fig. 10 (a) indicates that the voltage increases. The variations in the voltage have not been observed in this case of study. High magnitude of the sum absolute values curve at the time of switching off the resistive load indicates occurrence of the event. Hence, disturbances are observed in the voltage at PCC and power injected by the solar PV system into the smart grid during the switching off the inductive-resistive load in the smart grid.

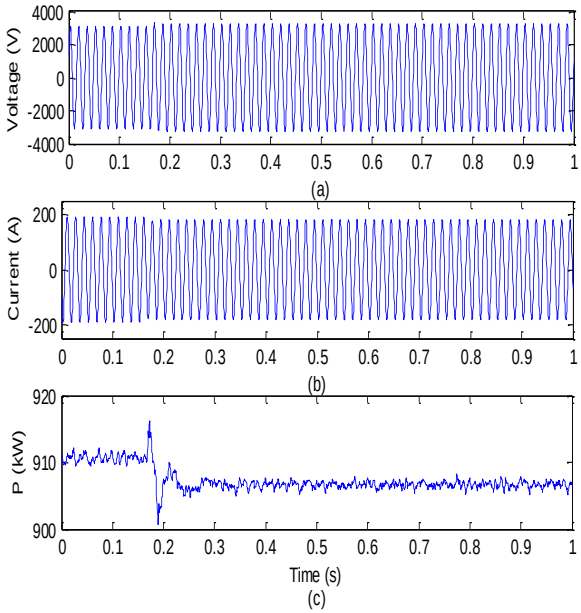

Fig. 9. (a) Voltage at PCC (b) current injected into the grid (c) active power flow with switching off the inductive resistive load in the presence of solar PV power generation

4.6 Switching on the Inductive-Resistive Load

The solar PV system of capacity 1 MW is integrated to the smart grid test system at the bus 680 and continuously injecting power into the smart grid test system. An inductive-resistive load of capacity 1155 kW and 1660 kVAr is switched on at 10th cycle from start of the simulation and integrated to the smart grid test system at PCC (bus 680). The voltage of phase-A at PCC, current injected into the grid at PCC by solar PV system and active power injected by the solar PV system in to the smart grid has been captured during the event of switching on the inductive-resistive load and their plots are shown in Figs. 12 (a), (b) and (c) respectively. Significant changes in the voltage and current visible by the naked eye are not observed as shown in Figs. 12 (a) and 12 (b) respectively. The power deviations of 15 kW have been observed for a period of 68 cycles as shown in Fig. 12 (c). It is also observed that power output of the solar PV system increases by an amount of 5 kW after switching on the inductive-resistive load.

IJASRM
International Journal of Advanced Scientific Research and Management, Volume 3 Issue 7, June 2018
www.ijasrm.com
ISSN 2455-6378

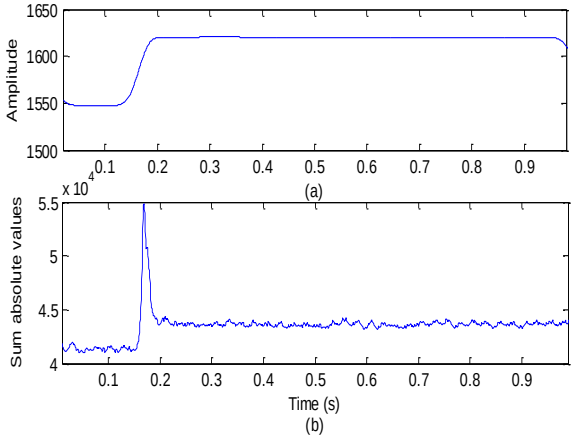

Fig. 10. Switching off the inductive resistive load in the presence of solar PV system (a) amplitude curve obtained from S-matrix (b) sum absolute values curve obtained from S-matrix

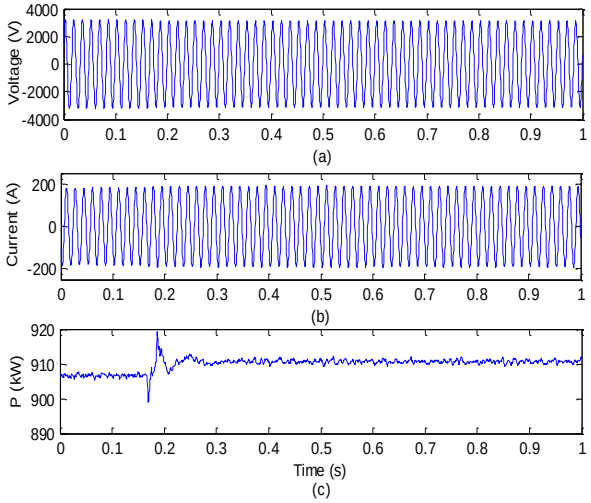

Fig. 11. (a) Voltage at PCC (b) current injected into the grid (c) active power flow with switching on the inductive resistive load in the presence of solar PV power generation

The amplitude curve and sum absolute values curve obtained from the S-matrix of the voltage during the switching on the inductive-resistive load are shown in Figs. 13 (a) and (b) respectively. The decrease in magnitude of amplitude curve after switching on the inductive-resistive load as shown in Fig. 13 (a) indicates that the voltage decreases after the operational event. High magnitude of the sum absolute values curve at the time of switching of the resistive load indicates occurrence of the event and presence of the disturbances. Hence, disturbances are observed in the voltage at PCC and power injected by the solar PV system into the smart grid during the switching on the inductive-resistive load in the smart grid.

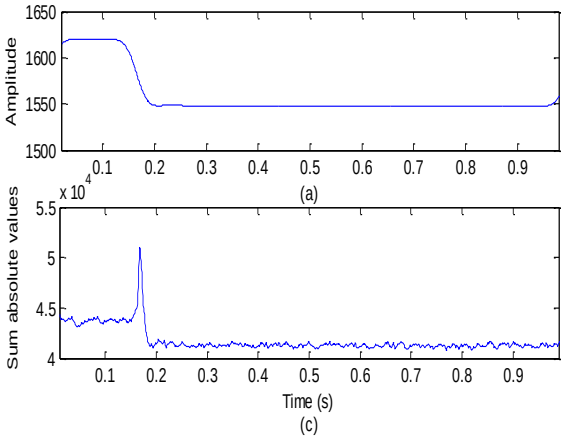

Fig. 12. Switching on the inductive resistive load in the presence of solar PV system (a) amplitude curve obtained from S-matrix (b) sum absolute values curve obtained from S-matrix

4.7 Switching on the Capacitor Bank

The solar PV system of capacity 1 MW is integrated to the smart grid test system at bus 680 and continuously injecting power into the smart grid test system. The capacitor bank of capacity 600 kVAr connected on the bus 675 is initially kept open circuited and switched on at 10th cycle from start of the simulation. The voltage of phase-A at PCC, current injected into the grid at PCC by solar PV system and active power injected by the solar PV system in to the smart grid have been captured during the event of switching on the capacitor bank and their plots are shown in Figs. 14 (a), (b) and (c) respectively. Significant changes in the voltage and current are observed as shown in Figs. 14 (a) and 14 (b) respectively. The power deviations of 40 kW have been observed for a period of 10 cycles as shown in Fig. 14 (c).

The amplitude curve and sum absolute values curve obtained from the S-matrix of the voltage during the switching on the capacitor bank are shown in Figs. 15 (a) and (b) respectively. The increase in the magnitude of amplitude curve after switching on the capacitor bank as shown in Fig. 15 (a) indicates that the voltage increases after the operational event. High magnitude of the sum absolute values curve at the time of switching of the capacitor bank indicates occurrence of the event and presence of the disturbances. Hence, disturbances are observed in the voltage at PCC and power injected by the solar PV system into the smart grid during the switching on the capacitor bank in the smart grid.

IJASRM
International Journal of Advanced Scientific Research and Management, Volume 3 Issue 7, June 2018
www.ijasrm.com
ISSN 2455-6378

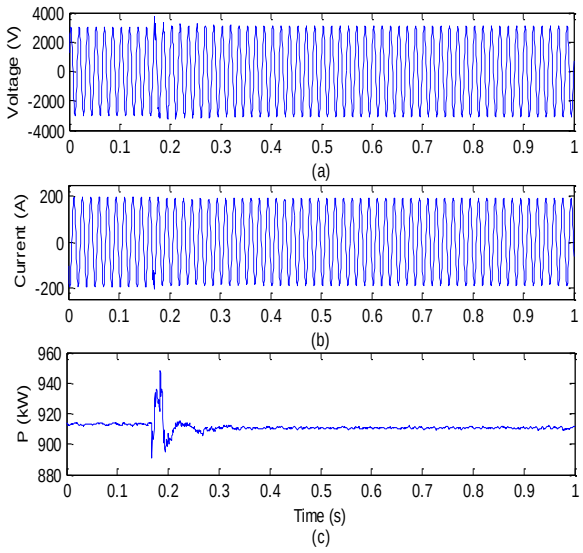

Fig. 13. (a) Voltage at PCC (b) current injected into the grid (c) active power flow with switching on the capacitor bank in the presence of solar PV power generation.

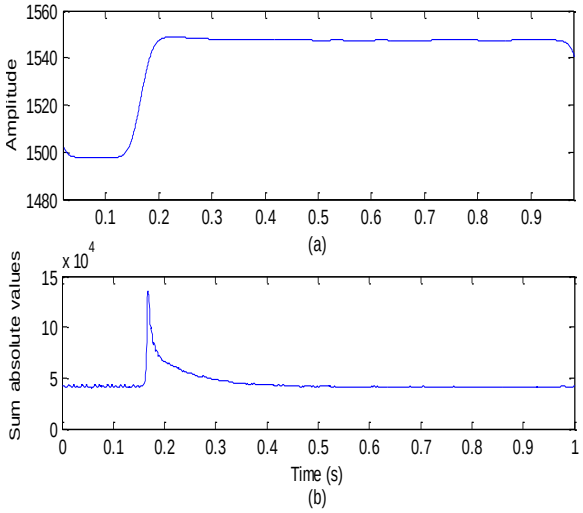

Fig. 14. Switching on the capacitor bank in the presence of solar PV system (a) amplitude curve obtained from S-matrix (b) sum absolute values curve obtained from S-matrix

4.8 Switching off the Capacitor Bank

The solar PV system of capacity 1 MW is integrated to the smart grid test system at bus 680 and continuously injecting power into the smart grid test system. The capacitor bank of capacity 600 kVAr connected on the bus 675 is switched off at 10^{th} cycle from start of the simulation. The voltage of phase-A at PCC, current injected into the grid at PCC by solar PV system and active power injected by the solar PV system in to the smart grid have been captured during the event of switching on the capacitor bank and their plots are shown in Figs. 16 (a), (b) and (c) respectively. Significant changes in the voltage and current are observed as shown in Figs. 16 (a) and 16 (b) respectively. The power deviations of 20 kW have been observed for a period of 6 cycles as shown in Fig. 16 (c).

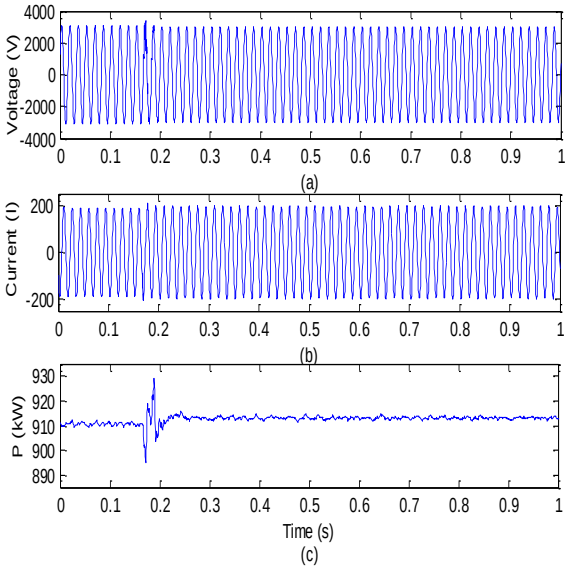

Fig. 15. (a) Voltage at PCC (b) current injected into the grid (c) active power flow with switching off the capacitor bank in the presence of solar PV power generation.

The amplitude curve and sum absolute values curve obtained from the S-matrix of the voltage during the switching off the capacitor bank are shown in Figs. 17 (a) and (b) respectively. The decrease in the magnitude of amplitude curve after switching off the capacitor bank as shown in Fig. 17 (a) indicates that the voltage decreases after the operational event. High magnitude of the sum absolute values curve at the time of switching off the capacitor bank indicates occurrence of the event and presence of the disturbances. Hence, disturbances are observed in the voltage at PCC and power injected by the solar PV system into the smart grid during the switching off the capacitor bank in the smart grid.

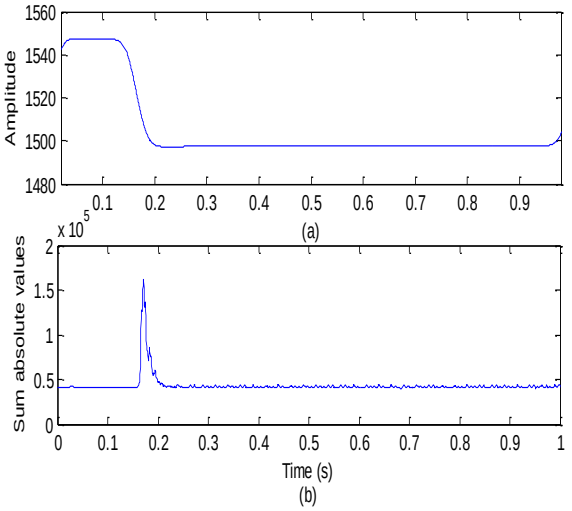

Fig. 16. Switching off the capacitor bank in the presence of solar PV system (a) amplitude curve obtained from S-matrix (b) sum absolute values curve obtained from S-matrix

The maximum values of parameters are provided in Table 2.

TABLE 1 Maximum Values of Parameters

S. No.	Case of study	Maximum value of sum absolute values curve	Maximum amplitude curve deviations (kW)	Maximum power deviations
1	Feeder tripping	$11x10^4$	+12, -12	+12
2	Feeder reclosing	$14x10^4$	+40, -20	-12
3	Switching off the resistive load	$5.9x10^4$	+5, -5	+18
4	Switching on the resistive load	$5.9x10^4$	+14, -14	-18
5	Switching off the resistive-inductive load	$5.5x10^4$	+5, -10	+65
6	Switching on the resistive-inductive load	$5.2x10^4$	+12, -10	-65
7	Switching off the capacitor load	$14x10^4$	+35, -25	+45
8	Switching on the capacitor load	$1.4x10^4$	+20, -15	-45

5 Conclusion

This paper presents a simple and effective technique for the detection of impacts of grid operations such as feeder tripping, feeder reclosing, switching on/off the resistive load, switching on/off the resistive-inductive load and switching on/off the capacitor bank on the output of the solar PV power system integrated to the smart grid. It is concluded that voltage affected more during the events of switching the loads and feeders as compared to the switching off the loads and feeders. Maximum effect on the voltage is observed with resistive-inductive load, followed by capacitor banks, resistive load and feeders. Effect on the output power is maximum with the inductive load, capacitor bank, feeders and resistive loads.

Reference

[1] Chanda S., De A., A multi-objective solution algorithm for optimum utilization of smart grid infrastructure towards social welfare. International Journal of Electrical Power Energy Systems, Vol. 58: 307-318 (2014).

[2] Claessen F. N., Claessens B., M. P. F., Molderink A., Bakker V., Toersche H. A., Broek M. A. van den, Comparative analysis of tertiary control systems for smart grids using the flex street model. Renewable Energy, Vol. 69: 260-270 (2014).

[3] Enrico De Santis, Lorenzo Livi, Alireza Sadeghian and Antonello Rizzi, Modelling and recognition of smart grid faults by a combined approach of dissimilarity learning and one-class classification. Neurocomputing, Vol. 170: 368–383 (2015).

[4] Evora J., Hernandez J. J., Hernandez M., A MOPSO method for direct load control in smart grid. Expert Systems with Applications, Vol. 42 (Issue 21): 7456-7465 (2015).

[5] Goulden M., Bedwell B., Rennick Egglestone S., Rodden T., Spence A., Smart grids, smart users, the role of the user in demand side management. Energy Research Social Science, Vol. 2: 21-29 (2014).

[6] Hu Q., Li F., Chen C. Fei, A smart home test bed for undergraduate education to bridge the curriculum gap from traditional power systems to modernized smart grids. IEEE Transactions on Education, Vol. 58 (Issue 1): 32-38 (2015).

[7] Karimi B., Namboodiri V., Jadliwala M., Scalable meter data collection in smart grids through message concatenation. IEEE Transactions on Smart Grid, Vol. 6 (Issue 4): 1697-1706 (2015).

[8] Liang J., Venayaga Moorthy G. K., Harley R. G., Wide-area measurement based dynamic stochastic optimal power flow control for smart grids with high variability and uncertainty. IEEE Transactions on Smart Grid, Vol. 3 (Issue 1): 59-69 (2012).

[9] Mahela, Om Prakash and Ola, Sheesh Ram, Impact of Grid Disturbances on the Output of Grid Connected Solar Photovoltaic System. 2016 IEEE Students' Conference on Electrical, Electronics and Computer Science, Bhopal, India (2016).

[10] Milioudis A. N., Andreou G. T., Labridis D. P., Enhanced protection scheme for smart grids using power line communications techniques, IEEE Transactions on Smart Grid, Vol. 3 (Issue 4): 1631-1640 (2012).

[11] Real, A. J. del, Arce, A., Bordons C., Combined environmental and economic dispatch of smart grids using distributed model predictive control. International Journal of Electrical Power Energy Systems,Vol. 54: 65-76 (2014).

[12] Sharma, Atul, Ola Sheesh Ram and Mahela, Om Prakash, Impact of Grid Disturbances on the Output of Grid Connected Wind Power Generation. 1st IEEE International Conference on Power Electronics, Intelligent Control and Energy Systems (ICPEICES-2015). New Delhi, India (2015).